# **COMMUNICATION**

# Phase field approach for nanoscale interaction between crack propagation and phase transformation

Hossein Jafarzadeh, a Valery I. Levitas, \*bc Gholam Hossein Farrahi \*a and Mahdi Javanbakht d

Received 00th January 20xx, Accepted 00th January 20xx

DOI: 10.1039/x0xx00000x

Phase field approach (PFA) to the interaction of fracture and martensitic phase transformation (PT) is developed, which includes change in surface energy during PT and the effect of unexplored scale parameter proportional to the ratio of the widths of the crack surface and the phase interface, both at nanometer scale. Variation of these two parameters causes unexpected qualitative and quantitative effects: shift of PT away from the crack tip, "wetting" of the crack surface by martensite, change in the structure and geometry of the transformed region, crack trajectory, and process of interfacial damage evolution, as well as transformation toughening. The results suggest additional parameters controlling coupled fracture and PTs.

Interaction between fracture and martensitic PTs is an extremely important problem in the physics and mechanics of strength, deformational, and transformational properties of materials. In particular, high stress concentration at the crack tip may cause PTs1-5. PT absorbs energy and also produces transformation strain, which serves as a mechanism of plastic deformation and stress relaxation. Both increase resistance to the crack growth and ductility, which is called transformation toughening. Also, stresses generated during PTs may cause fracture. PFA has been widely used for modeling the complex microstructure evolution such as fracture<sup>6-10</sup>, PTs<sup>11-15</sup>, and their interactions<sup>4, 16-20</sup>. However, only few works<sup>18-20</sup> consider both fracture and PT with the PFA. In the current letter, we significantly advance the PFA to coupled fracture and PT by integrating it with PFA to surface-induced pre-transformations and transformations and including a new nanoscale effect (see

We found through the simulations that the reduction in the surface energy during PTs promotes nucleation of M at the crack tip, its stabilization as a nanolayer at the crack surface, or nucleation of the pre-martensite or M at the crack surfaces. Increase in surface energy during PT suppresses the PT near the crack tip and at the surfaces, and stress-induced PT occurs slightly away from the crack tip. In turn, change in surface energy of a solid during PT affects crack behavior in terms of change in cohesion and gradient energy, which changes crack nucleation location and trajectory. All these changes are essentially affected by the dimensionless width  $\bar{\delta}$ .

The subscripts 0, d, A, and M are for the undamaged solid, fully-damaged solid, austenite, and martensite, respectively. The PT and damage are described by the order parameters  $\eta$  and  $\phi$ , respectively; both vary between zero and unity. The austenite (A) corresponds to  $\eta$ =0 and martensite (M) to  $\eta$ =1; the undamaged state is described by  $\phi$ =0 and fully damaged by  $\phi$ =1.

We consider PT between cubic austenite and tetragonal martensite in NiAl with transformation strain  $\varepsilon_t$ =(0.215,–0.078, –0.078)<sup>14</sup> and isotropic elasticity; other material parameters are given in the ESI. For these parameters, the width and energy of the phase interface are  $\delta_p = 5.54 \sqrt{\beta_0/(2A_0(\theta^e - \theta^c))}$ =1.5065nm and  $E = \sqrt{\beta_0 A_0(\theta^e - \theta^c)/18}$ =0.2245 N/m <sup>21</sup>. Isotropic surface energies  $\gamma_A$  and  $\gamma_M$  vary in the range of 0.5-5 N/m and are presented below as  $\bar{\gamma} = \gamma_M/\gamma_A$ . Flow chart of the methodology is given in Figure S1 (see ESI).

Electronic Supplementary Information (ESI) available: [details of any supplementary information available should be included here]. See DOI: 10.1039/x0xx00000x

ESI). PT<sup>13</sup> and fracture<sup>8</sup> are described with advanced models<sup>8, 13</sup>, which in contrast to previous models<sup>18, 19</sup>, satisfy some additional conditions to reproduce conceptually important features of stress-strain curves. Theory includes various coupling effects between fracture and PT. Thus, the suggested PFA is much more realistic than previous models<sup>18, 19</sup>. The key point is that the theory possesses two characteristic nanoscale parameters: widths of the crack surface  $\delta_c$  and the A-M interface width  $\delta_p$ . We consider parameter  $\bar{\delta}$  proportional to their ratio as the main dimensionless scale parameter in our formulation, and its effect is studied.

<sup>&</sup>lt;sup>a</sup> Sharif University of Technology, School of Mechanical Engineering, Tehran 11365-11155, Iran.

b. lowa State University, Departments of Aerospace Engineering and Mechanical Engineering, Ames, IA 50011, USA.

<sup>&</sup>lt;sup>c.</sup> Ames Laboratory, Division of Materials Science and Engineering, Ames, IA, USA. <sup>d.</sup> Isfahan University of Technology, Department of Mechanical Engineering, Isfahan

<sup>\*</sup> Corresponding authors: (VIL) email: <a href="mailto:vlevitas@iastate.edu">vlevitas@iastate.edu</a>; (GHF) email:

COMMUNICATION Journal Name

For the chosen cohesion energy  $\psi^c$ , the width of the crack surface  $\delta_c$  =1.14/8, where / is the initial distance between two planes forming crack surfaces. Thus, there are two characteristic widths, both at nanometer scale: width of the crack surface  $\delta_c$  (or I) and the A-M interface width  $\delta_p$ . We introduce  $\delta := 1.5(I/\delta_p)$  as the main dimensionless scale parameter in our theory. It was recently revealed that, for a free surface, such a ratio strongly affects the surface-induced martensitic  $PT^{21}$  and  $melting^{22}$  and is suggested as the new dimension in the phase diagram<sup>22</sup>. Generally, if any PFA includes two order parameters, their length scale ratio plays an essential role in the occurring different processes<sup>23</sup>, e.g. for interaction between PT and dislocations<sup>15</sup> and solid-solid PT via intermediate melt<sup>22</sup>. This parameter was never discussed for the fracture and, as is shown below, significantly affects PT and fracture processes. The plane stress problem is considered. Length, time, and stress dimensions were normalized by 1 nm, 1 ps, and 1 GPa, respectively.

**Pseudoelastic behavior.** Processes in a center cracked tension sample shown in Figure 1 are simulated at  $\theta/\theta^e$ =4.65, i.e. deeply in the austenitic region in the *pseudoelastic regime*. An initial crack (bold line at the center) is introduced via an analytical solution<sup>8</sup> for the damage parameter  $\phi$ . An initial value of  $\eta$ =0.001 is assumed everywhere. Homogeneous displacements u on the lateral edges are linearly increased to 1.125 nm in 0.075 ps and then remain constant. Due to the symmetry, only one-quarter of the sample is considered. Coupled PT and fracture are studied as function of  $\bar{\gamma}$  keeping  $\bar{\delta}$ = const and as a function of  $\bar{\delta}$  keeping  $\bar{\gamma}$ = const.

Figure 2 shows the distribution of  $\eta$  ahead of the moving crack tip. Traditionally, PT starts around the crack tip, where stress concentration is the highest 18, 19. Here, the martensitic region is determined not only by the stress concentration but also by  $\bar{\gamma}$  and  $\bar{\delta}$ . For  $\bar{\gamma} \leq 1$  M exists at the crack tip. However, for  $\bar{\gamma} = 10$  there is a residual A region around the crack tip with width  $\simeq \delta_c$ , because of its much lower surface energy. This is a new regime for the coupled crack and transforming zone propagation. Larger  $\bar{\delta} = 10$  increases the width of the A layer and suppresses martensitic PT, making M incomplete (premartensite) in the entire transforming zone, which is smaller than for  $\bar{\delta} = 1$ .

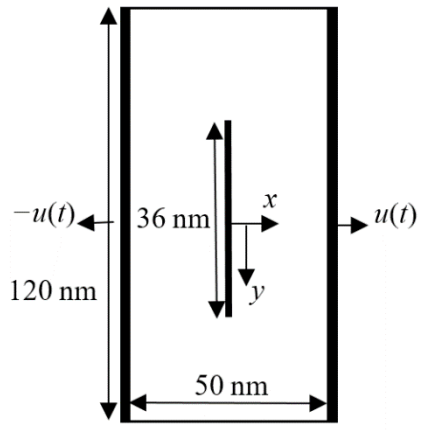


**Figure 1.** Schematics of the center cracked tension sample with the boundary conditions.

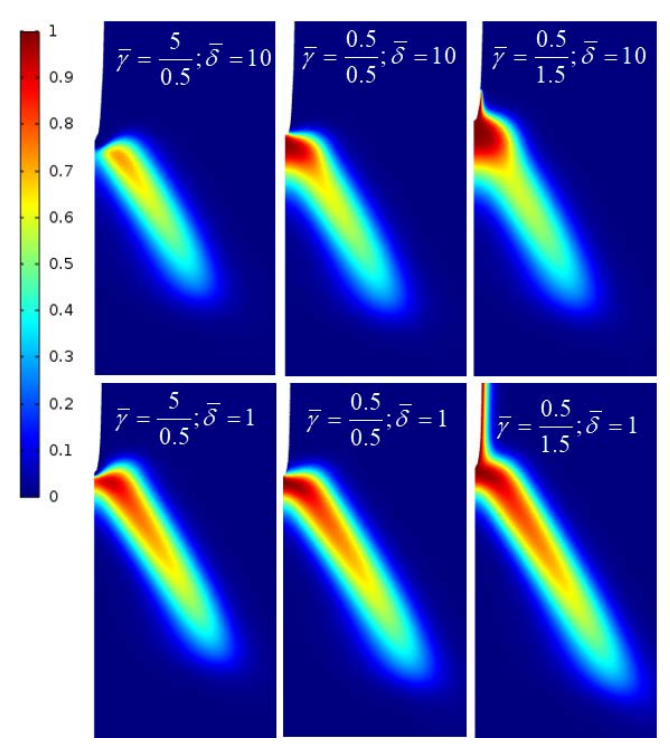


**Figure 2.** PT region described by the distribution of the order parameter  $\eta$  ahead of the moving crack tip at time t=2, shown in the region [x,y]=[(0, 10), (25, 45)] for different  $\overline{\gamma}$  and  $\overline{\delta}$  (shown in figures) for the pseudoelastic regime. The region with  $\phi$ ≥0.99 is eliminated from the figures and is shown as the crack.

For  $\overline{\gamma} = 1$ , the martensitic region is larger and transformation is more complete than for  $\bar{\gamma}=10$ . For both cases, the martensitic structure moves together with the crack tip, and the material undergoes direct and reverse PTs due to pseudoelastic behavior. Such a behavior is typically observed in an experiment for a pseudoelastic material which has a crack<sup>5</sup>. For  $\bar{\gamma}=1/3$ , the martensitic region grows further and resides at the crack surface, promoted by reduction of the surface energy during PT. For the thicker crack surface, M cannot propagate far away from the stress concentrator, but for the thinner crack surface, M propagates along the entire crack surface, i.e. "wets" it. This thin M layer is induced and stabilized by the surface after unloading deep in the region of stability of A. Such a residual M at crack and notch surfaces were observed experimentally for NiTi single crystal<sup>2</sup>. Thus, the traditionally-neglected scale parameter  $\delta$  essentially affects martensitic PT at the crack tip and crack propagation.

**Pseudoplastic behavior.** Similar problems are solved to study *pseudoplastic* behavior at  $\theta = \theta^e$  for which residual M exists after local unloading. We changed the barrier parameter  $A_0$  to keep the same barrier height  $\overline{A}$  and, consequently, the magnitude of the stress for the direct PT (see ESI for definitions of the material parameters).

In Figure 3 for  $\bar{\gamma}=1$ , when the surface energy does not have any contribution to the driving force for PT, the PT starts at the crack tip and the transformed region grows with the crack propagation, i.e. reverse PT does not occur behind the crack tip. This corresponds to known experiments 1. For  $\bar{\gamma}=10$ , smaller surface energy of A drives the reverse PT near the crack tip. This is a new effect for stress-induced PT during crack growth for the

Journal Name COMMUNICATION

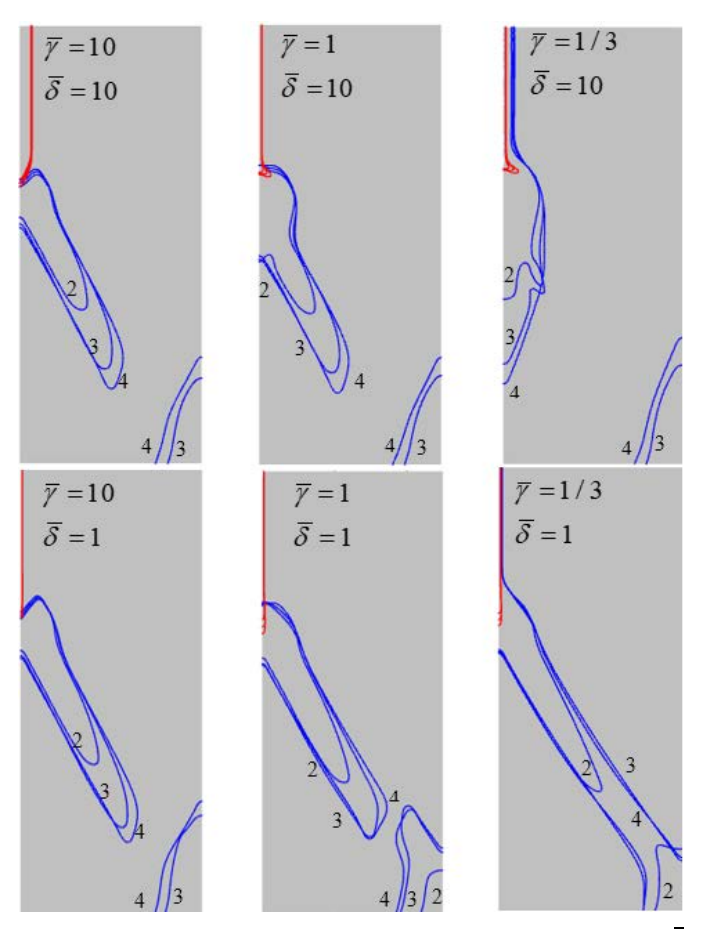


**Figure 3.** PT region (distribution of  $\eta$ ) ahead of the moving crack tip for different  $\overline{\gamma}$  and  $\overline{\delta}$  for the pseudoplastic regime. Red and blue lines show contour lines  $\phi$ =0.5 and  $\eta$ =0.5, respectively, for t=2, 3, and 4 (shown near curves).

pseudoplastic regime. For  $\bar{\gamma} \leq 1$ , the reverse PT does not occur; in addition, reduction of the surface energy leads to a surface-induced martensitic PT along the entire crack surface. Our results also show significant effects of the scale parameter  $\bar{\delta}$ . For  $\bar{\gamma}=10$ , there is a residual austenite region around the crack tip, and smaller  $\bar{\delta}$  results in the larger transformed region. However, in contrast to the pseudoelastic regime, martensitic PT is completed in the entire transformed region. For  $\bar{\gamma} \leq 1$ , the morphology of the transformed regions is entirely different for different  $\bar{\delta}$ . For larger  $\bar{\delta}$ , there is more M near the crack tip and along the crack surface and less in the growing-in-bulk-M plate. Promotion of the M by thicker crack surface relaxes stresses, suppressing martensite growth in the plate. Also, crack branching is observed for larger  $\bar{\delta}$ .

Interfacial fracture. Here we solve the problem for the same geometry and boundary conditions, shown in Figure 4, but the right side of the sample is initially martensite, i.e. interfacial crack is considered at  $\theta=\theta^e$ . The M was introduced by means of the analytical solution for the equilibrium interface<sup>14</sup>. A tensile misfit strain of 0.215 in M produces significant vertical compressive stress in M and tensile stress in A. To avoid the A $\leftrightarrow$ M PT and focus on the interfacial crack propagation, we used  $L_\eta << L_\phi$ , where  $L_\phi$  and  $L_\eta$  are the kinetic coefficients for damage and PT, respectively. Results will be also interpreted in terms of Griffith theory for crack propagation,

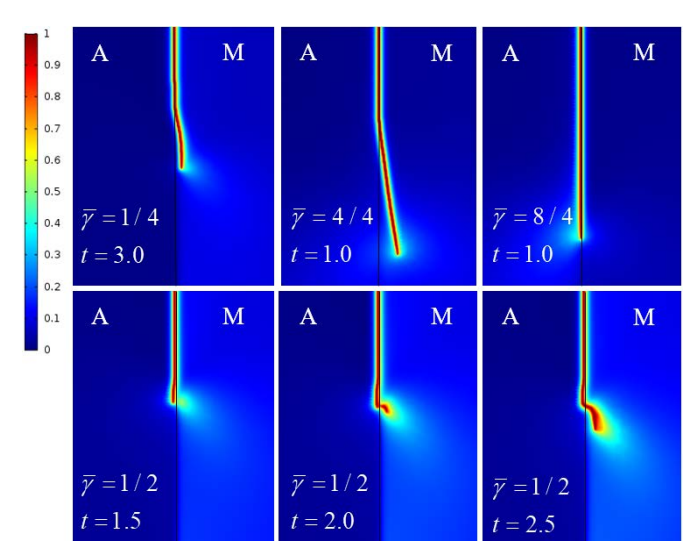


**Figure 4.** Damage distribution  $\phi$  within and outside the phase interface shown in the region [x,y]=[(-10 10),(25 50)] for  $\bar{\delta}$ =1 and different conditions shown in figures.

 $J>\Delta\gamma$  with  $\Delta\gamma=2\gamma_{\rm M}$  or  $2\gamma_{\rm A}$  or  $\Delta\gamma=\gamma_{\rm M}+\gamma_{\rm A}-E$ , (1) where J is elastic energy release, and three options for the change in surface energy of a crack  $\Delta\gamma$  are for crack propagating through M, A, or A-M interface, respectively.

Despite the symmetry in the loading and geometry, the crack path is not straight. For  $\bar{\gamma}=1/4$ , the crack deviates to the martensitic region due to much smaller  $\Delta \gamma$ . For  $\bar{\gamma}=1/2$ , the crack is initially directed to the A driven by tensile stresses due to misfit strain, i.e. by larger J despite the larger  $\Delta \gamma$ . Relaxation of internal stresses due to misfit and generation of tensile stresses near the crack tip leads to significant damage in the weaker M. Next, crack turns and propagates in the M, governed by smaller  $\Delta \gamma$ . For  $\bar{\gamma}=4/4$ , when  $\gamma_{\mathrm{M}}=\gamma_{\mathrm{A}}\gg E$  , termination of the lattice misfit at the crack surfaces produces a stress field and *J*, which lead to a deviation of the crack into M. For  $\bar{\gamma} = 8/4$ , larger  $\gamma_{\rm M}$  suppresses this deviation, leading to the interfacial crack propagation. Thus, interplay between initial stresses due to a lattice misfit at the A-M interface and different surface energies of A and M result in different crack propagation scenarios.

**Crack nucleation.** To study crack nucleation in Figure 5, the finite-width A-M interface was introduced using the analytical solution, but transformation strain was neglected. An initial value of  $\phi$ =0.01 is applied. The upper edge of a sample and the notch surface are stress-free; the right side is moved with u(nm)=2t(ps), the left side is fixed in the horizontal direction, and the lower left corner point is fixed. Vertical displacement at the lower horizontal plane is zero (v=0). Eq. (1) will be utilzed for the interpretation of the results.

For cases (a) and (b), the lowest  $\Delta \gamma$  in equation  $J > \Delta \gamma$  leads to barrierless crack nucleation and propagation in A and along the interface, respectively. For case (a), the lower surface energy of A leads to crack nucleation and propagation in A, even though disappearance of interface energy increases the driving force for crack growth within the interface. For cases (b)-(d), energies of A and M are equal. For case (b), the stress concentrator due to notch and the disappearance of the interface energy both lead to crack nucleation along the interface. In case (c), the effect of interface energy on the crack driving force is neglected, leading to larger  $\Delta \gamma$ ;

COMMUNICATION Journal Name

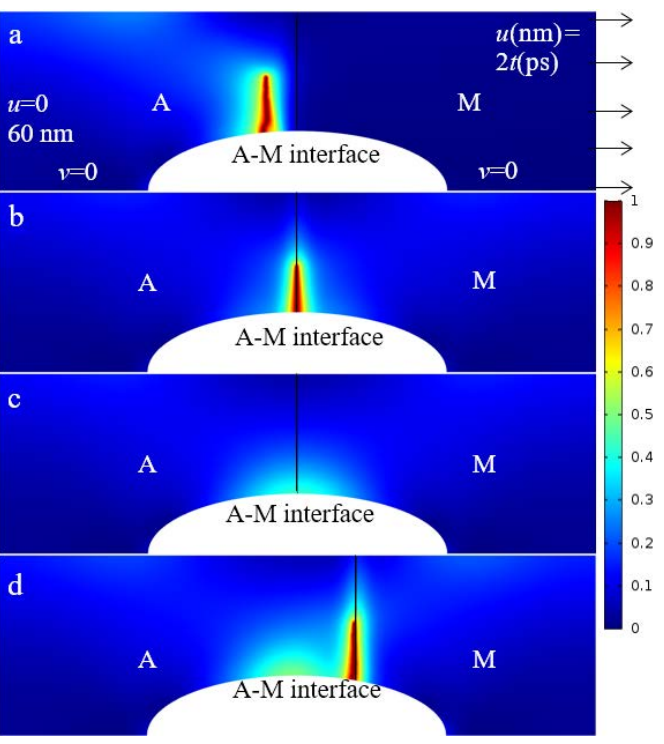


**Figure 5.** Damage distribution  $\phi$  within/near the phase interface for: a)  $\overline{\gamma}=5/0.5, t=2.8$ ; b)  $\overline{\gamma}=0.5/0.5, t=2.5$ ; c)  $\overline{\gamma}=0.5/0.5, t=2.5$ , without interface energy ( $A_0=\beta_0=0$  in Eq. (12) in ESI), and d)  $\overline{\gamma}=0.5/0.5, t=2.8$ . The interface ( $\eta=0.5$ ) is shown by a solid black line in each figure.

thus, for the same loading as in case (b), the crack does not nucleate. For case (d), while the stress concentration due to notch and J are larger in the middle of the sample than at the interface, the disappearance of interface energy is dominant, and the crack propagates through the interface due to smaller  $\Delta \gamma$ . Again, interplay between stress concentration, different surface energies of A and M, and disappearance of the energy of the pre-existing A-M interface produce variety of crack nucleation and evolution developments.

Transformation toughening. The easiest way to evaluate the transformation toughening is by comparing crack tip velocity for the cases without PT and different PT scenarios. This is collected in Table 1 for simulations in Figure 2 in pseudoelastic regime. Due to the complex and nonlinear interplay of all parameters involved in the Ginzburg-Landau equations, there is no straightforward relationship between the extension of PT in Figure 2 and the results in Table 1. For all cases, PT significantly reduces crack speed. The largest transformation toughening is for  $\bar{\gamma}=10$ , when A is located at the crack tip and surfaces; the second largest crack velocity reduction is for  $\bar{\gamma}=1/3$ , when M "wets" part of the entire crack surface; and the smallest influence of PT is for  $\bar{\gamma}=1$ . The largest effect of the parameter  $\bar{\delta}$  is within 9% for  $\bar{\gamma}=10$ ; this effect is nonmonotonous.

	$\overline{\gamma} = \frac{5}{0.5}$	$\overline{\gamma} = \frac{0.5}{0.5}$	$\overline{\gamma} = \frac{0.5}{1.5}$	no PT, γ <sub>A</sub> =0.5 N/m
$\overline{\delta} = 10$	1.13	1.33	1.19	1.82
$\overline{\mathcal{S}} = 5$	1.03	1.26	1.20	1.82
$\overline{\delta} = 1$	1.05	1.29	1.22	1.82

Table 1. Crack tip velocity for different cases (nm/ps)

#### Conclusions

An advanced PFA to the interaction between fracture and martensitic PT is developed with nontrivial couplings, explicitly incorporating surface-induced PT and pretransformation as well as the scale effect related to the ratio of the width of the crack surface to the width of the phase interface. It was demonstrated that the effect of these parameters on the PT and fracture is quite strong and multifaceted. In particular, lower surface energy of M than of A can cause surface-induced PT and pretransformation at the crack surface ("wetting" by martensite) even in the pseudoelastic regime, when unloading near the crack surface should cause the reverse PT. In contrast, lower surface energy of A than of M suppresses the PT at the crack tip and shifts M away from the region of the highest stress concentration in the pseudoelastic regime, and causes reverse PT to A at the crack tip in the pseudoplastic regime. The geometry and internal structure of the transformed region strongly depend on the parameter  $\bar{\delta}$  in both regimes. Parameters  $\bar{\gamma}$  and  $\bar{\delta}$  essentially affect crack trajectory (branching) and the process of interfacial damage evolution, as well as transformation toughening, i.e. these are new parameters controlling coupled fracture and PTs, and probably twinning <sup>24, 25</sup>.

Two different interpretations of the widths of interfaces and surfaces are used in the phase-field approach. In one of them, they are just regularization parameters without physical meaning. Our results show that the regularization lengths cannot be chosen arbitrarily because their ratio significantly affects the results of simulations. Alternatively<sup>14, 21-23, 26, 27</sup>, these are actual nanometer-size widths of interfaces, surfaces, intermediate phases within interfaces, dislocation bands, and pretransformed layers, which are determined using atomistic simulations and experiments. For example, for surface melting of Al nanoparticles,  $\bar{\delta}$  was determined by fitting phase-field approach results to the size-dependent melting temperature <sup>22</sup>. Widths of surface disordered/molten layer and of intermediate phases are determined as well  $^{26,\ 28,\ 29}.$  For this case, the obtained results represent real physical effects. For surface-induced martensitic transformations, widths of surface layer and surface energies of A and M are unknown<sup>4</sup>. These parameters, as well as width and energy of A-M interface, depend on composition, point defect segregation, dislocation structure at external surfaces and interfaces, and can be partly controlled. Note that phase interface width in Si can be changed from a

nanometer to infinity (i.e., leading to a homogeneous interface-free transformation) by applying special triaxial stresses<sup>5</sup>. We hope that our theoretical predictions will attract experimental efforts to determine material parameters and study predicted phenomena. Review article<sup>23</sup> is devoted solely to the effect of  $\delta$  in various material processes. Note that the results of phase-field approach to surface-induced martensitic phase transformations<sup>21</sup> and obtained surface structures may be

#### Conflicts of interest

observed at the crack surfaces as well.

The authors declare no competing financial interest.

Journal Name COMMUNICATION

### **Acknowledgements**

HJ acknowledges the support of Sharif University of Technology, Nano Foundation and Ministry of Science, Research and Technology of Iran. VIL acknowledges the support of the ONR (N00014-19-1-2082), NSF (DMR-1904830), ARO (W911NF-17-1-0225), and ISU (Vance Coffman Faculty Chair Professorship).

#### References

- U. D. Hangen and G. Sauthoff, *Intermetallics*, 1999, 7, 501-510.
- A. Creuziger, L. J. Bartol, K. Gall and W. C. Crone, *Journal of the Mechanics and Physics of Solids*, 2008, 56, 2896-2905.
- S. Gollerthan, M. L. Young, K. Neuking, U. Ramamurty and G. Eggeler, *Acta Materialia*, 2009, 57, 5892-5897.
- M. Mamivand, M. Asle Zaeem and H. El Kadiri, Acta Materialia, 2014, 64, 208-219.
- G. M. Vasko, Ph.D. Thesis, University of Minnesota, Minnesota, 2001.
- A. Karma, D. A. Kessler and H. Levine, *Physical Review Letters*, 2001, 87, 045501.
- 7. H. Henry and H. Levine, *Physical Review Letters*, 2004, **93**, 105504.
- 8. V. I. Levitas, H. Jafarzadeh, G. H. Farrahi and M. Javanbakht, International Journal of Plasticity, 2018, 111, 1-35.
- 9. G. H. Farrahi, M. Javanbakht and H. Jafarzadeh, *Continuum Mechanics and Thermodynamics*, 2018, DOI: 10.1007/s00161-018-0685-z.
- H. Jafarzadeh, G. H. Farrahi and M. Javanbakht, Continuum Mechanics and Thermodynamics, 2019, DOI: 10.1007/s00161-019-00775-1, 1-13.
- Y. M. Jin, A. Artemev and A. G. Khachaturyan, *Acta Materialia*, 2001, 49, 2309-2320.
- T. Lookman, A. Saxena and R. C. Albers, *Physical Review Letters*, 2008, 100, 145504.
- V. I. Levitas and D. L. Preston, *Physical Review B*, 2002, **66**, 134206.
- 14. V. I. Levitas, D. L. Preston and D.-W. Lee, *Physical Review B*, 2003, **68**, 134201.
- 15. V. I. Levitas and M. Javanbakht, *Nanoscale*, 2014, **6**, 162-
- 16. A. Boulbitch and A. L. Korzhenevskii, *The European Physical*
- Journal B, 2016, **89**, 261.

  17. A. Boulbitch, Y. M. Gufan and A. L. Korzhenevskii, *Physical*
- Review E, 2017, 96, 013005.
   R. Schmitt, C. Kuhn, R. Skorupski, M. Smaga, D. Eifler and R.
- Müller, Archive of Applied Mechanics, 2015, **85**, 1459-1468.
- 19. T. Zhao, J. Zhu and J. Luo, *Engineering Fracture Mechanics*, 2016, **159**, 155-173.
- J. Clayton and J. Knap, Continuum Mechanics and Thermodynamics, 2018, 30, 421-455.
- 21. V. I. Levitas and M. Javanbakht, *Physical Review Letters*, 2011, **107**, 175701.
- V. I. Levitas and K. Samani, *Physical Review B*, 2014, **89**, 075427.
- 23. V. I. Levitas, *Scripta Materialia*, 2018, **149**, 155-162.
- J. D. Clayton and J. Knap, Acta Materialia, 2013, 61, 5341-5353.

 J. D. Clayton and J. Knap, Computer Methods in Applied Mechanics and Engineering, 2016, 312, 447-467.

- B. Pluis, D. Frenkel and J. F. van der Veen, Surface Science, 1990, 239, 282-300.
- 27. V. I. Levitas and M. Javanbakht, *Physical Review Letters*, 2010, **105**, 165701.
- 28. J. Luo, *Critical reviews in solid state and materials sciences*, 2007, **32**, 67-109.
- B. Pluis, A. D. Van der Gon, J. Frenken, van der Veen and JF, *Physical Review Letters*, 1987, 59, 2678.
- V. I. Levitas, H. Chen and L. Xiong, *Physical Review Letters*, 2017, **118**, 025701.

# **Supporting Information**

# Phase field approach for nanoscale interaction between crack propagation and phase transformation

Hossein Jafarzadeh<sup>a</sup>, Valery I. Levitas<sup>b,c\*</sup>, Gholam Hossein Farrahi<sup>a#</sup>, Mahdi Javanbakht<sup>d</sup>

Emails: \*vlevitas@iastate.edu, #farrahi@sharif.edu

# 1. The total system of equations for interaction between crack propagation and phase transformation

We denote contractions between tensors  $A = \{A_{ij}\}$  and  $B = \{B_{ij}\}$  as  $A \cdot B = \{A_{ij}B_{jk}\}$ ,  $A : B = A_{ij}B_{ji}$ , and  $A \otimes B = A_{ij}B_{kl}$ . The subscripts 0, d, A, and M are for the undamaged solid, fully-damaged solid, austenite, and martensite, respectively. The PT and damage are described by the order parameters  $\eta$  and  $\phi$ , respectively; both vary between zero and unity.  $\eta$  is the order parameter which describes phase transformation; The austenite (A) corresponds to  $\eta = 0$  and martensite M to  $\eta = 1$ .  $\phi$  is the order parameter which describes damage; the undamaged state is described by  $\phi = 0$  and fully damaged by  $\phi = 1$ . The crack surface with a narrow width in which the material is partially broken is described by  $0 < \phi < 1$ . Equations related to PTs, fracture, and surface-induced PTs alone are most close to those presented in the previous models<sup>1-3</sup>, respectively.

The relationship between strain  $\varepsilon$ , displacement u, and decomposition of the strain into elastic  $\varepsilon_e$  and transformational  $\varepsilon_t f(\eta)$  parts are

$$\boldsymbol{\varepsilon} = 0.5 (\nabla \boldsymbol{u} + \nabla \boldsymbol{u}^T) = \boldsymbol{\varepsilon}_e + \boldsymbol{\varepsilon}_t f(\eta); \tag{S1}$$

$$f(\eta) = a\eta^2 + (4 - 2a)\eta^3 + (a - 3)\eta^4. \tag{S2}$$

<sup>&</sup>lt;sup>a</sup> Sharif University of Technology, School of Mechanical Engineering, Tehran 11365-11155, Iran

<sup>&</sup>lt;sup>b</sup> Iowa State University, Departments of Aerospace Engineering and Mechanical Engineering, Ames, IA 50011, USA

<sup>&</sup>lt;sup>c</sup> Ames Laboratory, Division of Materials Science and Engineering, Ames, IA, USA

<sup>&</sup>lt;sup>d</sup> Isfahan University of Technology, Department of Mechanical Engineering, Isfahan 84156-83111, Iran

<sup>\*, #</sup> To whom correspondence should be addressed.

The interpolation function f is justified<sup>1</sup> and satisfies f(0) = 0, f(1) = 1, and f'(0) = f'(1) = 0 and will be used for any material property. This allows one to ensure that  $\eta = 0$  and  $\eta = 1$  are the thermodynamic equilibrium values of  $\eta$  for any temperature and stresses. The Helmholtz free energy is

$$\psi = \psi^e + \psi^f + \psi^{PT}; \quad \psi^f = \psi^c + \psi^{\nabla}_{\phi}; \quad \psi^{PT} = \psi + \psi + \psi^{\nabla}_{p}, \tag{S3}$$

where  $\psi^f$  and  $\psi^{PT}$  are the fracture and PT energy.

Elastic energy has the form

$$\psi^{e} = 0.5(1 - \phi)^{2} \boldsymbol{\varepsilon}_{e} : \boldsymbol{C}_{0} : \boldsymbol{\varepsilon}_{e} ; \quad \boldsymbol{C}_{0} = \boldsymbol{C}_{A} + (\boldsymbol{C}_{M} - \boldsymbol{C}_{A}) f(\eta),$$
(S4)

where  $C_0$  is the tensor of elastic moduli. Isotropic elasticity is used for simplicity, for which tensors  $C(C_A \text{ and } C_M)$  have the following structure

$$\boldsymbol{C} = (K_0 - \frac{2}{3}G_0)\boldsymbol{I} \otimes \boldsymbol{I} + 2G_0\boldsymbol{I}_4,$$
(S5)

where  $G_0$  and  $K_0$  are shear and bulk moduli, I is the second-order identity tensor, and  $I_4$  is the symmetric fourth-order identity tensor.

Cohesion energy is

$$\psi^{c} = \frac{2\gamma(\eta)}{l(\eta)} f(\phi); \quad \gamma(\eta) = \gamma_{A} + (\gamma_{M} - \gamma_{A}) f(\eta);$$

$$l(\eta) = l_{A} + (l_{M} - l_{A}) f(\eta); \quad l_{M} - l_{A} = \mathbf{n} \cdot \boldsymbol{\varepsilon}_{t} \cdot \mathbf{n} l_{A},$$
(S6)

where  $\gamma(\eta)$  is the specific isotropic surface energy, l is the initial distance between two planes forming crack surfaces, and  $\mathbf{n} = \nabla \phi / |\nabla \phi|$  is normal to this plane. Change in surface energy during the PT from its value for A  $\gamma_A$  to that for M  $\gamma_M$  is explicitly included in the formulation. This integrates our PFA to fracture and PTs with PFA to surface-induced PTs and pretransformations<sup>4</sup>, which was not previously applied to fracture. We use the advanced expression for  $\gamma(\eta)^6$ , which, in contrast to the other models<sup>4, 5</sup>, allows for the non-contradictory description of the equilibrium states at the surface.

Gradient energies for crack  $\psi^{\,
abla}_{\,\phi}$  and PT  $\psi^{\,
abla}_{\,\eta}$  are

$$\psi_{\phi}^{\nabla} = 0.5 \beta_{\phi}(\eta) |\nabla \phi|^2; \qquad \beta_{\phi}(\eta) = 0.612 \gamma(\eta) l(\eta); \tag{S7}$$

$$\psi_n^{\nabla} = 0.5 \beta_n(\phi) |\nabla \eta|^2; \quad \beta_n(\phi) = \beta_0 + (\beta_d - \beta_0) f(\phi),$$

where the expression for  $\beta_{\phi}(\eta)$  is taken from <sup>2</sup>.

The double-well barrier function for PT is

$$\widetilde{\psi} = \overline{A}\eta^2 (1 - \eta)^2; \quad \overline{A} = A(\theta - \theta^c);$$

$$A = A_0 + (A_d - A_0) f(\phi); \quad \theta^c = \theta_0^c + (\theta_d^c - \theta_0^c) f(\phi),$$
(S8)

where  $\theta^c$  is the critical temperature at which stress-free A loses its thermodynamic stability,  $\overline{A}$  is the barrier for transformation between A and M and A is material parameter.

Chemical part of the free energy  $\tilde{\psi}$  is

$$\tilde{\psi} = \Delta G^{\theta} f(\eta), \ \Delta G^{\theta} = -\Delta s^{e}(\theta - \theta^{e});$$

$$\Delta s^{e} = \Delta s_{0}^{e} + (\Delta s_{d}^{e} - \Delta s_{0}^{e}) f(\phi); \ \theta^{e} = \theta_{0}^{e} + (\theta_{d}^{e} - \theta_{0}^{e}) f(\phi),$$
(S9)

where  $\theta^e$  is the thermodynamic equilibrium temperature for stress-free A and M and  $\Delta s^e$  is the jump in specific entropy at  $\theta^e$ . Analyzing analytical solutions for the A-M interface<sup>7</sup> and the crack surface <sup>2</sup>, we accept for a specific model:

$$A_d = 0; \quad \theta^c = \theta_0^c = \theta_d^c; \quad \beta_d = 0; \quad \Delta s^e = \Delta s_0^e = \Delta s_d^e,$$
  
and  $\theta^e = \theta_0^e = \theta_d^0; \quad l(\eta) = l_A := l.$  (S10)

These assumptions, in particular, imply that the A-M interface energy vanishes during damage. We also assume a=0 for interpolation of  $\tilde{\psi}^{-1}$  and a=3 for  $\psi^{c-2}$  and all other parameters.

Stress tensor is defined by the Hooke's law:

$$\boldsymbol{\sigma} = \frac{\partial \psi}{\partial \boldsymbol{\varepsilon}} = (1 - \phi)^2 \boldsymbol{C}_0 : \boldsymbol{\varepsilon}_e. \tag{S11}$$

Ginzburg-Landau equations are

$$\frac{1}{L_{\eta}} \frac{\partial \eta}{\partial t} = -\frac{\partial \psi}{\partial \eta} \Big|_{\varepsilon} + \nabla \cdot \frac{\partial \psi}{\partial \nabla \eta} = 
6\eta (1 - \eta) \boldsymbol{\sigma} : \boldsymbol{\varepsilon}_{t} - 3\eta (1 - \eta) (1 - \phi)^{2} \boldsymbol{\varepsilon}_{e} : (\boldsymbol{C}_{M} - \boldsymbol{C}_{A}) : \boldsymbol{\varepsilon}_{e} - 
12\eta^{2} (1 - \eta) \Delta G^{\theta} - 2(1 - 3\phi^{2} + 2\phi^{3}) \eta (1 - \eta) \times (1 - 2\eta) A_{0} (\theta - \theta^{c}) - 
3\eta (1 - \eta) \left[ \frac{4(\gamma_{M} - \gamma_{A})}{l} (3\phi^{2} - 2\phi^{3}) + (\beta_{M} - \beta_{A}) |\nabla \phi|^{2} \right] + \nabla \cdot \left[ \beta_{0} (1 - 3\phi^{2} + 2\phi^{3}) \nabla \eta \right];$$
(S12)

$$\frac{1}{L_{\phi}} \frac{\partial \phi}{\partial t} = -\frac{\partial \psi}{\partial \phi} \Big|_{\mathcal{E}} + \nabla \cdot \frac{\partial \psi}{\partial \nabla \phi} =$$

$$(1 - \phi)\mathcal{E}_{e} : C_{0} : \mathcal{E}_{e} + 3\phi(1 - \phi) \Big[ 2A_{0}(\theta - \theta^{c})\eta^{2}(1 - \eta)^{2} + \beta_{0} |\nabla \eta|^{2} \Big] -$$

$$\frac{12}{I} \phi (1 - \phi) \Big[ \gamma_{A} + (\gamma_{M} - \gamma_{A})(3\eta^{2} - 2\eta^{3}) \Big] + \nabla \cdot \Big\{ \Big[ \beta_{A} + (\beta_{M} - \beta_{A})(3\eta^{2} - 2\eta^{3}) \Big] \nabla \phi \Big\},$$
(S13)

where  $L_{\phi}$  and  $L_{\eta}$  are the kinetic coefficients;  $L_{\phi}=0$  when the crack is under closing compressive stresses<sup>2</sup>. In such a way we exclude crack propagation under closing stresses. This is a stricter approach<sup>2</sup> than to exclude some parts of elastic energy, which are related to the compressive stresses/strains, from the driving force for crack propagation<sup>8</sup>.

Coupled system of Eqs. (1)-(13) (some of them are included in the extended version of Eqs. (12)-(13)) along with equilibrium equations  $\nabla \cdot \boldsymbol{\sigma} = \boldsymbol{\theta}$  and boundary conditions for the order parameters,  $\boldsymbol{n} \cdot \partial \psi / \partial \nabla \eta = 0$  and  $\boldsymbol{n} \cdot \partial \psi / \partial \nabla \phi = 0$ , are solved using the finite-element method and COMSOL code. A flow chart for the problem formulation and solution is presented in Fig. S1.

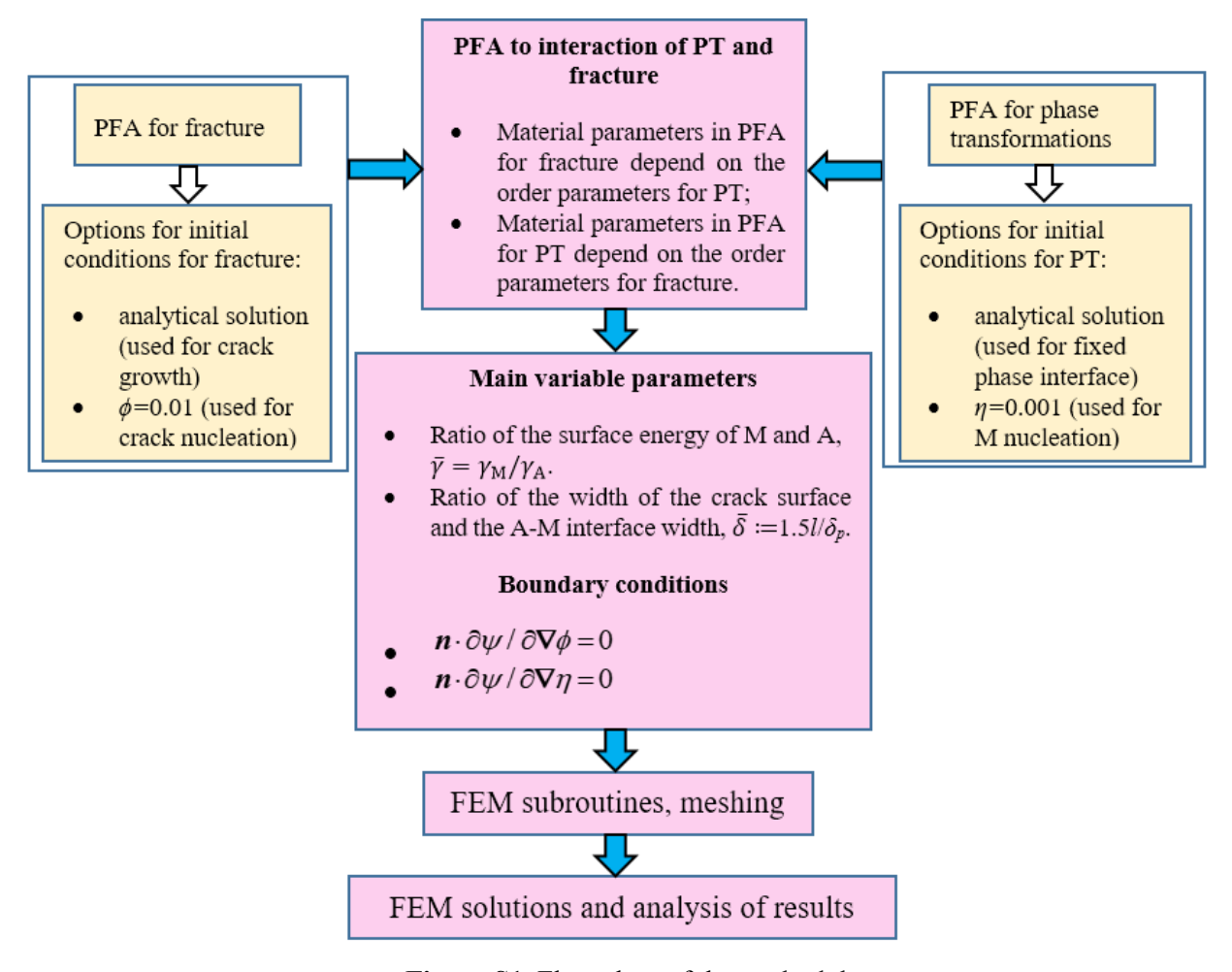


**Figure S1.** Flow chart of the methodology

### 2. Material Parameters

We consider phase transformation between cubic austenite and tetragonal martensite in NiAl associated with the transformation strain  $\varepsilon_t$ . All material parameters are collected in Table S1.

**Table S1.** Material parameters and their physical meaning

Definition/physical meaning	Value from the literature <sup>7</sup> unless otherwise stated
Isotropic bulk modulus (the same for austenite and martensite)	<i>K</i> <sub>0</sub> =112.62 GPa
Isotropic shear modulus (the same for austenite and martensite)	$G_0 = 71.5 \text{ GPa}$
Transformation strain from cubic austenite to tetragonal martensite	$\varepsilon_t = (0.215, -0.078, -0.078)$
Double well barrier parameter between the austenite and martensite	A <sub>0</sub> =4.40 MPa/K
Gradient energy coefficient for the phase transformation	$\beta_0 = 5.18 \times 10^{-10} \mathrm{N}$
Phase equilibrium temperature for the stress-free austenite and martensite	$\theta^e$ =215 K
Critical temperature at which stress-free A loses its thermodynamic stability	$\theta^c = -183 \text{ K}$
Energy of phase interphase	E=0.2245 N/m
Kinetic coefficients for phase transformation	$L_{\eta}$ =2596.5 (P a·s) <sup>-1</sup>
Kinetic coefficients for fracture (assumed from the accepted range <sup>2</sup> )	$L_{\phi} = 1000 (\text{Pa·s})^{-1}$

# 3. Propagation of the interfacial crack

Here, the same problem is solved as in Figure 4 of the main text (i.e. evolution of the initial interfacial crack at  $\theta = \theta^e$ ), with all the same material parameters, including  $\overline{\gamma} = \gamma_M / \gamma_A$ , but both  $\gamma_A$  and  $\gamma_M$  are decreased by a factor of two. Results are generally close to those in Figure 4, but nonzero damage spreads over a large region around a secondary crack outside the interface, which is unexpected. However, this is not contradictory, because as our analysis<sup>2</sup> shows, most phase field models for fracture, including the current one, allow stable damage below the ultimate strength, which causes deviation of the stress-strain curve from the straight line. In our case, large stresses at the crack tip and due to termination of the lattice misfit at the crack's free surfaces became close to the ultimate strength of martensite due to the small chosen  $\gamma_M = 0.5$  N/m. This does not happen at  $\gamma_M = 1$  N/m due to the larger ultimate strength of martensite. Due to the smaller ultimate strength of martensite, the crack moves faster in Figure S2 than in Figure 4. Also, crack propagation is not

continuous. In Figure S2 (b), maximum damage in martensite is shifted from the crack tip in austenite due to smaller strength. After stress exceeds the ultimate strength of the martensite at this location, material instability starts and a new crack nucleates in Figure S2 (c). Next, both cracks coalesce and the resultant crack continues propagation in the martensite (Figure S2 (d)). Figure S2 (a) also shows the deviation of crack to martensite due to its smaller ultimate strength without new crack nucleation.

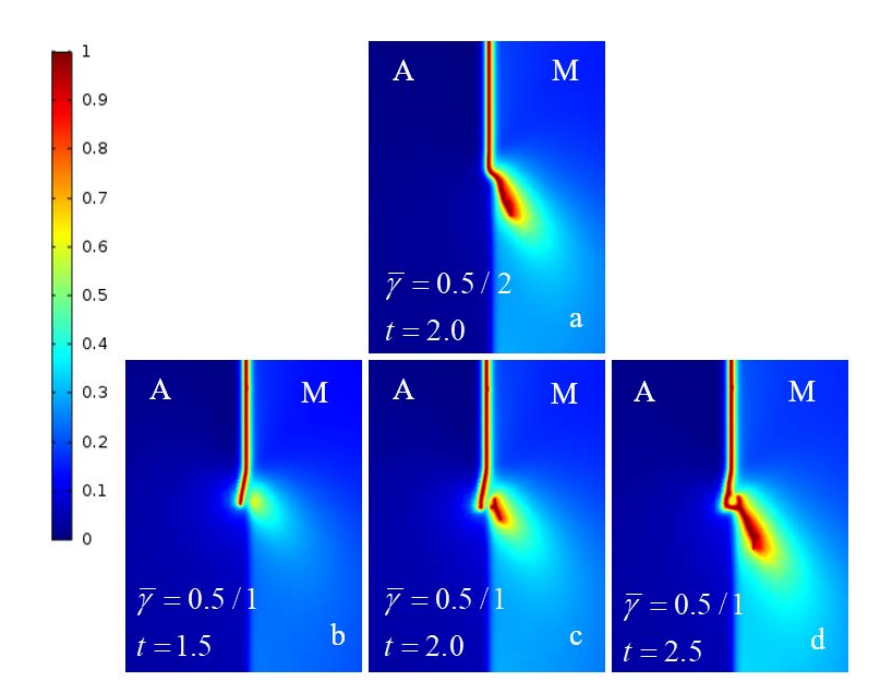


**Figure S2.** Damage distribution  $\phi$  within and outside the phase interface shown in the region  $[x,y]=[(-10\ 10),(25\ 50)]$  for l=1 and different conditions. (a) Damage at time t=2 for  $\overline{\gamma}=0.5/2$ ; (b) – (d) Damage evolution for times 1.5, 2.0, and 2.5 for  $\overline{\gamma}=0.5/1$ .

#### REFRENCES

- 1. V. I. Levitas and D. L. Preston, *Physical Review B*, 2002, **66**, 134206.
- 2. V. I. Levitas, H. Jafarzadeh, G. H. Farrahi and M. Javanbakht, *International Journal of Plasticity*, 2018, **111**, 1-35.
- 3. V. I. Levitas and M. Javanbakht, *Physical Review Letters*, 2011, **107**, 175701.
- 4. R. Lipowsky, *Physical Review Letters*, 1982, **49**, 1575-1578.
- 5. B. Pluis, D. Frenkel and J. F. van der Veen, *Surface Science*, 1990, **239**, 282-300.
- 6. V. I. Levitas and M. Javanbakht, *Physical Review Letters*, 2010, **105**, 165701.
- 7. V. I. Levitas, D. L. Preston and D.-W. Lee, *Physical Review B*, 2003, **68**, 134201.
- 8. R. Schmitt, C. Kuhn, R. Skorupski, M. Smaga, D. Eifler and R. Müller, *Archive of Applied Mechanics*, 2015, **85**, 1459-1468.